Circuit Modelling Methodology for Dual-band Planar Antennas

Kim Ho Yeap [1], Tobias Meister [2], Zi Xin Oh [1], and Humaira Nisar [1]

[1] Faculty of Engineering and Green Technology
Universiti Tunku Abdul Rahman, Jalan Universiti, Bandar Barat, 31900 Kampar, Perak, Malaysia
yeapkh@utar.edu.my, ohzixin@1utar.my, humaira@utar.edu.my

[2] Fakultät Angewandte Natur- und Kulturwissenschaften
Ostbayerische Technische Hochschule Regensburg, Postfach 12 03 27, 93025 Regensburg, Germany
tobias1.meister@st.oth-regensburg.de

Abstract ─ This paper presents a simple and systematic approach to determine the equivalent frequency-independent circuit model for a dual-band planar antenna. The Foster Canonical network synthesis technique with two RLC tanks has been employed to generate the two resonant bands of the antenna. The transfer function model is subsequently refined using a data fitting algorithm (viz the Nelder-Mead simplex algorithm). Parametric adjustments are performed at the final stage in order to further improve the accuracy of the final parameters.

Index Terms ─ Data-fitting algorithm, equivalent circuit, Foster canonical network, planar antenna, resonant bands.

I. INTRODUCTION

The continuous improvement in the design of planar printed antennas has contributed significantly to the technological advancement of wireless telecommunication. Prior to the mid-1990s, for instance, majority of the GSM handsets could only support single band operations [1]. In order to support more than one band, a few antennas are required to be installed into the device. Hence, the size of a multi-functional telecommunication device was usually bulky in those days. This is to say that; the functionalities of the device are very often traded for its size and portability. As dual-band antennas made their debut in 1996 [2 – 6], however, telecommunication devices experienced a dramatic reduction in sizes. With its ability to support multiple bands using a single antenna, much space has therefore been spared. Since then, researchers have been exploring ways to enhance the number of bands supported by an antenna; while, at the same time, making sure that its size is constrained within certain permissible dimensions [7 – 13].

When designing an antenna, it is important to derive its lumped equivalent circuit. This is because the circuit provides useful insights into the performance and operational principles of the antenna. It is also worthwhile noting that antennas are usually designed using electromagnetic field solvers, such as HFSS [14] or CST [15]; whereas, the receiver circuits are usually designed using electronic circuit simulators, such as SPICE [16]. Hence, the equivalent circuit of an antenna is useful when integrating the antenna with the front-end receiver circuits, during the validation phase. Validating both the antenna and receiver as a whole will certainly provide better accuracy to the actual performance of the system.

Antennas which generate only one resonant band can be easily modelled as a serial or parallel connection of resistance (R), inductance (L), and capacitance (C). When two or more bands are involved, however, the equivalent circuit turns out to be more complicated. In [17], Foster proposed modelling the resonant bands using RLC tanks, such as those shown in Fig. 1. The number of RLC tanks (represented by the subscript n) in the figure corresponds to the resonant bands that the circuit could generate. Thereafter, different methods, which adopt Foster's network synthesis technique as the cornerstone of their work, have been developed to derive the RLC equivalent circuit of antennas [18 – 22]. Since the Foster canonical network consists of various lumped passive elements, it is usually challenging to determine the exact combination of parameters which fits the return loss curve. As can be seen in the literature [18 – 22], the procedures applied to determine the parameters are usually quite laborious and mathematically involved.

In this paper, a simple and systematic approach to determine the equivalent circuit model for a dual-band planar antenna is presented. The derivation of the parameter for each element in the Foster canonical network is progressively described. We shall demonstrate that the return loss obtained from the approximate approach agrees reasonably well with that from an electromagnetic solver. In order to improve the accuracy

of the circuit, the parameters are refined using a data fitting algorithm and then parametrically fine-tuned at the final stage of the design.
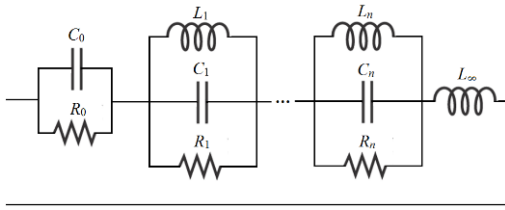

Fig. 1. General circuit topology of the Foster canonical network.

II. EQUIVALENT CIRCUIT TOPOLOGY

Besides the radiating resonant modes which are described by the *RLC* tanks in the Foster canonical network, quasi-static fields are present in an antenna as well. As can be seen in Fig. 1, these fields are characterized by the combination of resistance R_0, capacitance C_0 and inductance L_∞ in the circuit network. The resistance R_0 accounts for the conduction loss of the substrate material; whereas, the asymptotic behaviour of the feed point impedance at the higher and lower edges of the antenna frequency band is modelled by C_0 and L_∞ [23]. The quasi-static inductance L_∞ is usually infinitesimal when the order of the resonant modes is low. Hence, the circuit network for a dual-band antenna can be simplified into that in Fig. 2. The input impedance Z_{in} in the figure can be expressed as:

$$Z_{in} = \frac{1}{\frac{1}{R_0}+sC_0} + \frac{1}{\frac{1}{R_1}+\frac{1}{sL_1}+sC_1} + \frac{1}{\frac{1}{R_2}+\frac{1}{sL_2}+sC_2}, \quad (1)$$

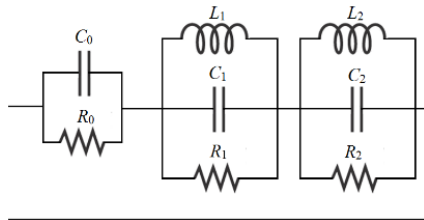where $s = j2\varpi f$ and f is the operating frequency.

Fig. 2. The circuit topology for a dual-band antenna.

III. NUMERICAL EXAMPLE

To carefully outline the procedure in determining the lumped elements in the antenna, a dual-band monopole antenna designed using HFSS is used as an example. The planar antenna is connected to a microstrip feedline and is printed on an FR4-epoxy substrate which has a thickness of 1.6 mm, dielectric constant of 4.4 and loss tangent of 0.022. As can be seen from the layout in Fig. 3, the antenna is composed of two rectangular radiating patches. Since a monopole antenna exhibits optimal performance when its length is a quarter of its

operating wavelength λ, the lengths of the top and bottom patches have been, respectively, kept to be within a quarter wavelength of the first and second resonant frequencies. As can be seen from the return loss curve in Fig. 4, the antenna resonates at f_{r1} = 2.1 GHz and f_{r2} = 5.2 GHz and it constitutes 15 dB bandwidths of 1.05 GHz (from 1.75 to 2.80 GHz) and 0.6 GHz (from 4.84 to 5.44 GHz) for the lower and upper resonant bands, respectively. Both resonant bands cover various IEEE 802.11 wireless local area network (WLAN) channels, which include those within the 2.4 GHz, 5.2 GHz, 4.9 GHz, 5.0 GHz, and 5.8 GHz bands.

Upon close inspection on the circuit topology in Fig. 2, it can be seen that the quasi-static resistance R_0 and capacitance C_0 can be readily evaluated from [19]:

$$R_0 = \lim_{f \to 0^+} Re\{Z_{in}(f)\}, \quad (2)$$

and

$$C_0 = \lim_{f \to 0^+} \frac{Im\{Y_{in}(f)\}}{2\pi f} = \frac{1}{2\pi}\lim_{f \to 0^+}\frac{\partial Im\{Y_{in}(f)\}}{\partial f}, \quad (3)$$

where Y_{in} is the input admittance of the circuit. Figures 5 and 6 depict, respectively, the simulated input resistance and susceptance of the antenna as a function of frequency. As f approaches 0, it can be seen that R_0 and C_0 can be approximated as 15 Ω and 0 F, respectively.

In comparison with the resistance, the magnitude of the susceptance turns out to be considerably smaller. This result suggests that both the non-static inductance (i.e., L_1 and L_2) and capacitances (i.e., C_1 and C_2) are much smaller than the resistance (i.e., R_1 and R_2). In order to estimate the parameters of the *RLC* tanks, values close to the 50 Ω characteristic impedance Z_0 are arbitrarily assigned to resistance R_1 (i.e., 30 Ω) and R_2 (i.e., 50 Ω); whereas, both C_1 and C_2 are arbitrarily set to 2 pF. The resonant frequency f_r of a simple parallel *RLC* network is given in (4) below:

$$f_r = \frac{1}{2\pi \times \sqrt{LC}}. \quad (4)$$

Inductance L_1 and L_2 can therefore be easily found by substituting the corresponding capacitance (i.e., C_1 and C_2) and resonant frequencies (i.e., f_{r1} and f_{r2}) into (4). The return loss *RL* of the circuit can be calculated by substituting (1) into (5) below:

$$RL = -20\log\left(\left|\frac{Z_{in}-Z_0}{Z_{in}+Z_0}\right|\right). \quad (5)$$

Figure 7 shows the comparison of the return loss curves computed from (5) and that obtained from the simulation. In order to investigate the effect of the curve at the presence of C_0, we have also plotted the return loss with C_0 arbitrarily chosen at 3 pF. Despite observing deviations among the curves, it is apparent that the theoretical results register certain resemblance with the simulation. In particular, the curve plotted based on the absence of C_0 are closer to that obtained from the simulation at the resonant frequencies f_r. To improve the accuracy of the parameters, a non-linear data fitting algorithm, such as the Nelder-Mead simplex optimization

routine, is adopted to minimize the mean-square error between both results. In this case, the approximate parameters for the lumped elements are used as the initial guesses for the search. Since eight parameters are involved in the optimization process, it is clearly not easy for the solution to converge to the required roots. Hence, it is often necessary to perform parametric adjustments on the parameters to further refine the accuracy of the results. The return loss curve, computed using the final parameters (shown in Table 1), is compared with the simulation result, as shown in Fig. 8. It is apparent from the figure that both curves are now in good agreement with each other. In fact, the *RLC* network resonates at the same frequencies and magnitudes with those generated from the planar antenna and both curves are highly correlated at the second band.

IV. CONCLUSION

A simple and systematic approach to evaluate the parameters in the Foster canonical network is presented here. The circuit network provides insight into the passive elements existing in a dual-band planar antenna. The approach starts with an approximation from the input resistance and susceptance of the antenna. The combination of parameters is subsequently refined so that the network could give a more realistic behaviour of the actual antenna.
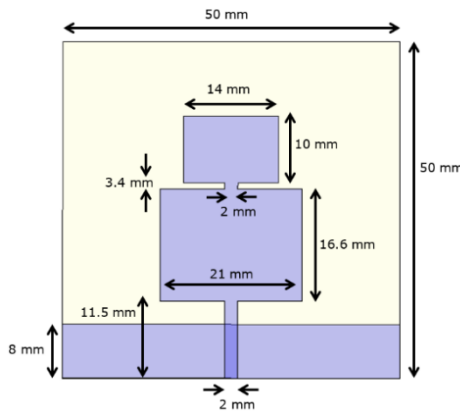

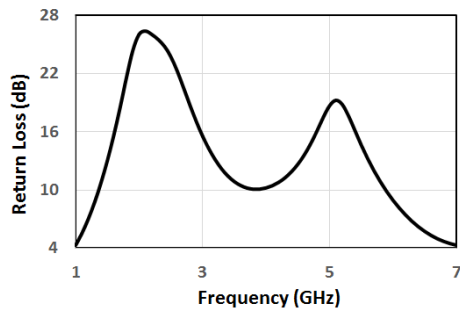Fig. 3. The layout of a dual-band planar antenna.

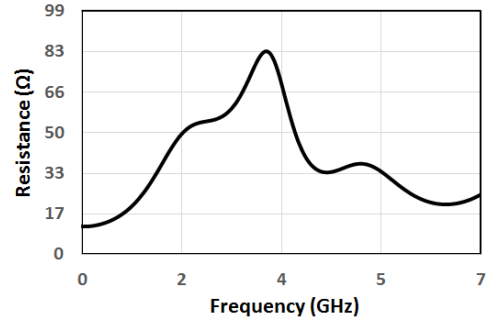Fig. 4. The simulated return loss of a planar antenna.

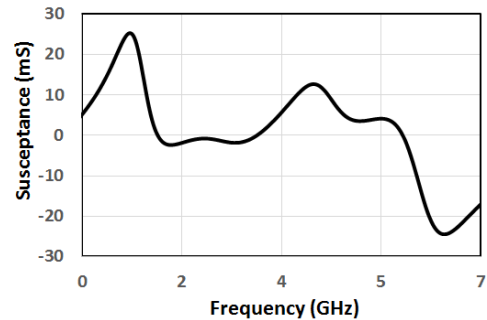Fig. 5. The input resistance of a planar antenna.

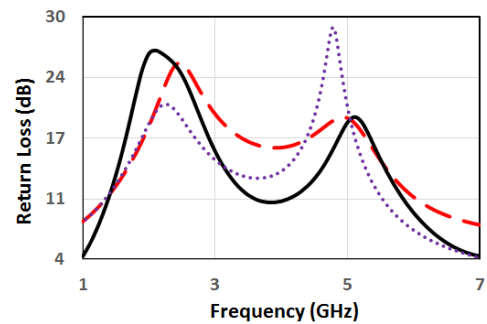Fig. 6. The input susceptance of a planar antenna.

Fig. 7. The return loss obtained from the simulation (solid line) and the initial parameters with $C_0 = 0$ F (dashed line) and $C_0 = 3$ pF (dotted line).
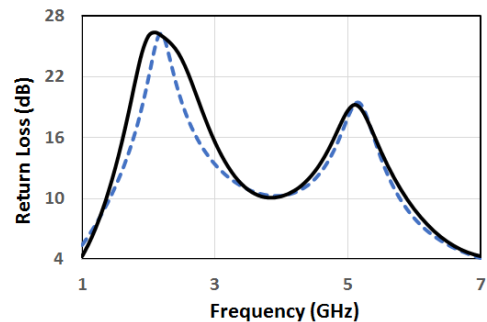

Fig. 8. The return loss obtained from the simulation (solid line) and final parameters (dotted line).

Table 1: Lumped elements in an antenna

Component	Value
R_0	1.3 Ω
C_0	0 F
R_1	54.1 Ω
C_1	1.36 pF
L_1	5.1 nH
R_2	66.5 Ω
C_2	1.66 pF
L_2	0.48 nH

REFERENCES

[1] C. Rowell and E. Y. Lam, "Mobile-phone antenna design," *IEEE Antennas and Propagat. Magazine*, vol. 54, no. 4, pp. 14-34, Aug. 2012.

[2] Z. Ying, "Progress of multiband antenna technology in mobile phone industry," *IEE Wideband and Multi-band Antennas and Arrays*, Birmingham, UK, Sep. 7, 2005.

[3] Z. Ying, "Multi-band non-uniform helical antennas," *1996-IO (granted first in USA)*, US006122102, WO-9815028.

[4] I. Egorov and Z. Ying, "A non-uniform helical antenna for dual band cellular phones," *IEEE Antennas and Propagat. Society Int. Symp.*, Salt Lake City, USA, July 16-21, 2000.

[5] P. Haapalg and P Vainikainen, "Helical antennas for multi-mode mobile phones," *26th European Microwave Conf.*, Prague, pp. 327-331, 1996.

[6] G. J. Hayes, "Dual band meander antenna," *US-0459553*, WO-WS08058, 1996.

[7] K. H. Yeap, C. S. Voon, T. Hiraguri, and H. Nisar, "A compact dual-band implantable antenna for medical telemetry," *Microwave and Opt. Technol. Lett.*, vol. 61, pp. 2105-2109, July 2019.

[8] C. S. Voon, K. H. Yeap, K. C. Lai, C. K. Seah, and H. Nisar, "A compact double-psi-shaped dual band patch antenna for WLAN/LTE applications," *Microwave and Opt. Technol. Lett.*, vol. 60, pp. 1271-1275, Apr. 2018.

[9] A. Altaf and M. Seo, "A tilted-D-shaped monopole antenna with wide dual-band dual-sense circular polarization," *IEEE Antennas and Wireless Propagat. Lett.*, vol. 17, no. 12, pp. 2464-2468, 2018.

[10] W. L. Yeo, K. C. Lai, K. H. Yeap, P. C. Teh, and H. Nisar, "A compact-dual band hook-shaped antenna for wireless applications," *Microwave and Opt. Technol. Lett.*, vol. 59, no. 8, pp. 1882-1887, Aug. 2017.

[11] L. Adam, M. N. M. Yasin, H. A. Rahim, P. J. Soh, and M. F. Abdulmalek, "A compact dual-band rectenna for ambient RF energy harvesting," *Microwave Opt. Technol. Lett.*, vol. 60, pp. 2740-2748, 2018.

[12] H. R. Cheong, K. H. Yeap, K. C. Lai, P. C. Teh, and H. Nisar, "A compact CPW-fed antenna with S-shaped patches for multiband applications," *Microwave and Opt. Technol. Lett.*, vol. 59, no. 3, pp. 541-546, Mar. 2017.

[13] K. H. Yeap, W. L. Yeo, K. C. Lai, T. Hiraguri, K. Hirasawa, and Z. X. Oh, "A compact E-shaped antenna with C-shaped slots and a back-patch for multiband applications," *J. of Electrical Engineering*, vol. 71, no. 1, pp. 49-54, Feb. 2020.

[14] High Frequency Structure Simulation (HFSS), Ansys, Inc., Canonsburg, PA.

[15] CST Studio Suite, Dassault Systèmes Simulia Corp., Providence, Rhode Island.

[16] Simulation Program with Integrated Circuit Emphasis (SPICE), University of California, Berkeley, California.

[17] R. M. Foster, "A reactance theorem," *Bell Syst. Tech. J.*, vol. 3, no. 2, pp. 259-267, Apr. 1924.

[18] K. H. Sayidmarie and L. S. Yahya, "Modeling of dual-band cresecent-shape monopole antenna for WLAN applications," *Int. J. of Electromagnetics and Applications*, vol. 4, no. 2, pp. 31-39, 2014.

[19] D. Caratelli, N. Haider, and A. Yorovoy, "Analytically based extraction of Foster-like frequency-independent antenna equivalent circuits," *Proc. of the Int. Symp. on Electromagnetic Theory*, Hiroshima, Japan, pp. 506-509, May 20-24, 2013.

[20] O. K. Heong, C. K. Chakrabarty, and G. C. Hock, "Circuit modeling for rectangular printed disc monopole antenna with slot for UWB system," *Proc. of the 3rd Int. Conf. on Intelligent Sys. Modelling and Simulation*, Kota Kinabalu, Malaysia, pp. 727-731, Feb. 8-10, 2012.

[21] S. B. T. Wang, A. M. Niknejad, and R. W. Brodersen, "Circuit modeling methodology for UWB omnidirectional small antennas," *IEEE J. on Selected Areas in Communications*, vol. 24, no. 4, pp. 871-877, Apr. 2006.

[22] T. Ali, K. D. Prasad, and R. C. Biradar, "A miniaturized slotted multiband antenna for wireless applications," *J. of Computational Electronics*, vol. 17, pp. 1056-1070, 2018.

[23] M. Ansarizadeh, A. Ghorbani, and R. A. Abd-Alhameed, "An approach to equivalent circuit modeling of rectangular microstrip antennas," *Progress in Electromagnetics Research B*, vol. 8, pp. 77-86, 2008.